

Full length article



Quantum-enhanced angle-of-arrival pre-estimation of radio-frequency signals

Wei Li ^{a,b}, Xiaocong Sun ^{a,c}, Yuhang Tian ^a, Fan Li ^a, Long Tian ^{a,b}, Yajun Wang ^{a,b}, Chuanliang Li ^c, Yaohui Zheng ^{a,b,*}

^a State Key Laboratory of Quantum Optics and Quantum Optics Devices, Institute of Opto-Electronics, Shanxi University, Taiyuan 030006, China

^b Collaborative Innovation Center of Extreme Optics, Shanxi University, Taiyuan, Shanxi 030006, China

^c Shanxi Engineering Research Center of Precision Measurement and Online Detection Equipment and Department of Physics, Taiyuan University of Science and Technology, Taiyuan, Shanxi 030024, China

ARTICLE INFO

Keywords:

Quantum metrology

Quantum sensing

Angle-of-arrival pre-estimation

ABSTRACT

Quantum metrology with quantum effects, gives remarkable possibility to increase the precision of estimated parameter. Here, we demonstrate a quantum-enhanced angle-of-arrival pre-estimation protocol, which conduces to predict a target orientation for modern phased-array radar and sonar systems. Taking edge sensor as reference, we estimate the first, second, and third derivatives of radio-frequency (RF) phase via only four-sensor network arranged in linear topology. Combining the quantum technology with high-order derivatives, the receiving angle-of-arrival at arbitrary sensor can be pre-estimated with enhanced sensitivity of nearly 49.5%.

1. Introduction

Quantum metrology, which leverages the quantum technique like entanglement, can yield fabulous quantum advantage over any classical approaches [1–3]. The ultimate precision of quantum metrology can reach the Heisenberg bound $1/N$ for noiseless scenario, outperforming the corresponding classical limit $1/\sqrt{N}$, where N is the number of probes [4–6]. Since first proposed in 1980s [7], significant advances have been made lately in numerous systems including neutral atoms [8], trapped ions [9,10], Rydberg atoms [11], solid-state [12], superconducting circuits [13] and photons [14]. Quantum-enhanced precision has been demonstrated for a multitude of physical quantities encompassing gravitational wave, electric fields, magnetic field, time and frequency, temperature, and pressure [15–18]. Recently, the precision of non-Markovian quantum metrology [19] was investigated by introducing the quantum Fisher information (QFI). Distribute quantum sensing, which leverages multipartite entangled states to boost the performance for estimating global properties by an array of sensors, significantly widens the applicable scenario of quantum metrology including phased-array radar, dark matter searches [20], absorption spectroscopy [21], strain monitoring of large buildings and mines.

Angle-of-arrival (AoA), an efficient way to determine the direction of the incoming radio-frequency (RF) signal, can be applied in wireless

communications [22], source localization, target tracking [23], astronomical observation, phased-array radar and sonar [24]. In the past twenty years, a multitude of photonic-based structures have been proposed and demonstrated to estimate the AoA of RF signal. To guarantee the estimation efficiency and simplify the configuration simultaneously, the receiving RF signals have been mapped to phase shift [25], time delay [26], electrical power [27–29], optical power [30], DC voltages [31], from which the phase information is extracted. Further, the estimation sensitivity of AoA is enhanced via quantum entanglement [32]. However, the scheme was achieved with only the first-order derivative of RF phase, which limits the phase estimation precision.

Pre-estimation of AoA, which is extensively applied in military weapon systems [33] such as an intercept warning receiver (INR) [34], is a significant step to reduce scanning range of a radar and provide preprocessing of large-scale sensor network. In this letter, we demonstrate an AoA pre-estimation of radio-frequency signals for arbitrary sensor via the existing four-partite entangled network. By utilizing diverse weights for quantum sensor network, the first, second and third derivatives of RF phase at edge sensor are directly estimated with noise reduction of above -5.2 dB. Taking edge sensor as reference, the AoA pre-estimation at arbitrary sensor arranged in linear topology can be realized according to the acquired derivatives, the estimation precision is far superior to that with only the first-order derivative.

* Corresponding author at: State Key Laboratory of Quantum Optics and Quantum Optics Devices, Institute of Opto-Electronics, Shanxi University, Taiyuan 030006, China.

E-mail address: yhzheng@sxu.edu.cn (Y. Zheng).

<https://doi.org/10.1016/j.optlastec.2023.109643>

Received 26 March 2023; Received in revised form 12 May 2023; Accepted 22 May 2023

Available online 6 June 2023

0030-3992/© 2023 Elsevier Ltd. All rights reserved.

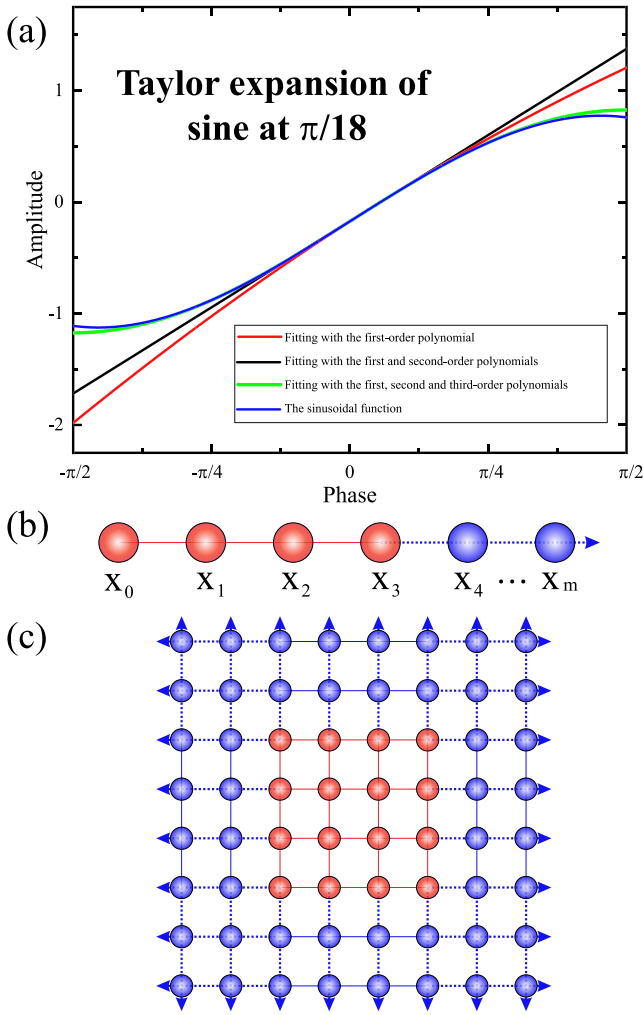


Fig. 1. Schematic diagram of AoA pre-estimation. (a) Taylor expansion of sinusoidal function about a reference point $\pi/18$. The black curve showcases the fitting result with only the first-order polynomial, the red (green) curve represents the fitting result with the first and second-order polynomials (the first, second and third-order polynomials). As the order number is increased, the phase estimation approaches sinusoidal function (blue curve) gradually. (b) Sensor array is arranged in linear topology. Taking edge sensor X_0 as reference, the phase shift at any sensor arranged in linear topology can be pre-estimated. (c) Sensor array can be extended to rectangular topology, similar to the linear one.

2. Experimental setup for phase noise suppression and characterization

Suppose the RF signal at the m th sensor is $E_m \cos(\Omega t + \varphi_m)$, where E_m , Ω , φ_m ($m = 0, 1, 2, 3$) are the amplitude, carrier frequency and phase respectively. Driven by the RF field, an electro-optic modulator (EOM) induces a displacement on the phase quadrature $\alpha_m = \varepsilon_m E_m \sin \varphi_m$, in which ε_m represent the radio frequency to photonics conversion coefficient. As described in [32], $\varepsilon_m = \frac{\pi \gamma}{V_c k}$ depends on the half-wave voltage of EOM and the amplitude of optical field at the m th sensor. It is difficult to measure RF phase directly, thus one can measure the displacement α_m and estimate the phase φ_m . According to Taylor expansion, the sinusoidal function cannot be reconstructed with only the first-order derivative of reference point, as shown in Fig. 1(a). At least the first, second and third-order polynomials are required to reconstruct the sinusoidal function with high precision.

Therefore, the first, second and third derivatives of RF phase at edge sensor X_0 should be firstly achieved, providing the coefficient for the polynomial estimating. High-order derivatives can be achieved

by the available four-sensor network. As shown in Fig. 1(b), the sensors are arranged in linear topology. The RF phase estimator under investigation is formulated as $\varphi = \sum_{j=0}^3 \beta_j \varphi_j$, where β_j and φ_j are the weights and estimated RF phase at each sensor. For specific estimation tasks, an appropriate multipartite entangled state should be tailored to maximize the sensitivity improvement, and the obtained minimum noise variances are expressed as $\delta^2 \varphi = \frac{\beta^2}{4} [\frac{\eta}{(\sqrt{N_s} + 1 + \sqrt{N_s})^2} + 1 - \eta]$, where $n_s = \frac{N_s}{4}$ is photon number, and $1 - \eta$ is the loss at each sensor [35–37]. By exploiting the finite difference method referring to the edge sensor X_0 [32], the optimum weights for the first, second and third derivatives are expressed as $\beta_0 : \beta_1 : \beta_2 : \beta_3 = -11/6 : 3 : -3/2 : 1/3$, $-2 : 5 : -4 : 1$ and $-1 : 3 : -3 : 1$, respectively.

After the first, second and third derivatives of the RF phase at edge sensor X_0 are experimentally obtained, we can pre-estimate the RF phase at arbitrary right sensor X_m arranged in linear topology, which is expressed as

$$\varphi_m = \varphi_0 + \varphi'_0 \Delta x_m + \frac{1}{2} \varphi''_0 \Delta x_m^2 + \frac{1}{6} \varphi'''_0 \Delta x_m^3 + o(\Delta x_m^4) \quad (1)$$

where Δx_m is the distance between the edge sensor X_0 and the m th sensor X_m . The relative phase difference between two sensors X_0 and X_m can be described as $\varphi_m - \varphi_0 = 2\pi k \Delta x_m \cos \theta / \lambda + 2n\pi$, where θ is the AoA, k and λ is the wave vector and wavelength of RF signal, and n is an integer. Then the AoA can be expressed as

$$\theta = \arccos \frac{\lambda(\varphi_m - \varphi_0 - 2n\pi)}{2\pi k \Delta x_m} \quad (2)$$

Therefore, the AoA θ between sensors X_0 and X_m can be pre-estimated by phase difference $\varphi_m - \varphi_0$ with credible value. Similarly, we can pre-estimate the AoA at left sensor with the sensor X_3 as the edge sensor. In this regard, the optimum weights should be tailored to $11/6 : -3 : 3/2 : -1/3$ for the estimation of the first derivative, $-2 : 5 : -4 : 1$ for the second derivative, and $1 : -3 : 3 : -1$ for the third derivatives, respectively.

Further, our proposal can be extended to a more general scenario with large-scale $N \times N$ sensor network, as shown in Fig. 1(c). By constructing a 4×4 quantum sensing network and estimating the first, second, third derivatives of RF phase at the four corner sensors, the AoA for arbitrary sensor in the two-dimensional sensor network can be pre-estimated with enough sensitivity. We expect that the AoA pre-estimation proposal can shorten scanning time, improve processing efficiency at a large-scale sensor network.

3. Experimental setup

As shown in Fig. 2, the experimental setup is divided into three parts: generation of phase squeezed state, RF sensor network and data acquisition. The squeezed state is generated by a sub-threshold optical parametric amplifier (OPA) whose architecture is semi-monolithic resonator consisting of a piezo-actuated output coupler and a PPKTP crystal [38–41]. One face of PPKTP crystal whose dimensions is 1 mm*2 mm*10 mm is polished with a radius of curvature of 12 mm, while the other face is a flat surface with AR coating for both wavelengths. The convex face of crystal has highly reflective (HR) coating for 1064 nm and anti-reflective coating for 532 nm, whereas the transmissivity of output coupler is 12% for 1064 nm, ensuring the reasonable escape efficiency and modest threshold. The radius of curvature for output coupler is 30 mm, and an air gap is 27 mm, guaranteeing that the waist spot is in the middle of crystal. According to stability condition and PPKTP crystal refractive index ($n = 1.81$), the cavity length of OPA is 37 mm, the corresponding linewidth is 94 MHz, and the fineness is 81. Without the injection of pump beam, the output of the OPA is coherent beam that serves as the light source of classical sensor networks. When the pump beam is injected, and the OPA operates in a parametric amplification status by locking the relative phase between seed beam and pump beam at 0,

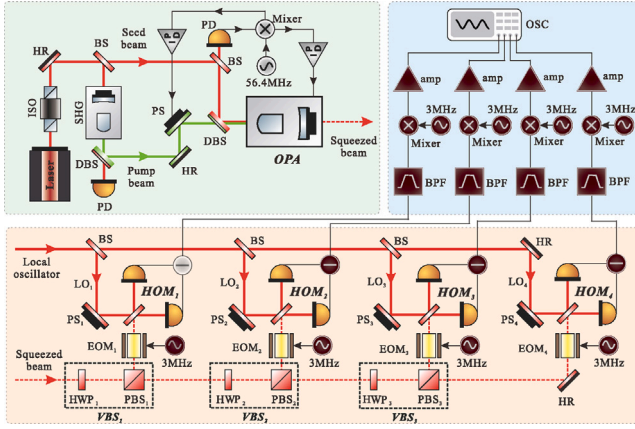


Fig. 2. Experimental setup of RF signal pre-estimation with a continuous variable entangled network. ISO: isolator; EOM: electro-optic phase modulator; HR: high reflectivity mirror; PD: photoelectric detector; BS: beam splitter; DBS: dichroic beam splitter; SHG: second harmonic generator; OPA: optical parametric amplifier; HWP: half-wave plate; PBS: polarization beam splitter; VBS: variable beam splitter; PS: phase shifter; HOM: homodyne detection; BPF: band-pass filter; amp: amplifier; OSC: oscilloscope.

the OPA generates a phase squeezed light to perform the measurements of entangled sensor networks. No experimental parameters other than the presence or absence of the pump beam are varied during the comparative measurement of the classical and entangled networks.

With the phase squeezed state, four-partite continuous variable (CV) entangled states are generated by a variable beam splitter (VBS) network that is composed of three pairs of half-wave plates (HWPs) and polarization beam splitters (PBSs). Contraposing different sensing tasks, the optimum weights for each sensor can be controlled by finely tuning the rotation angle of half-wave plate so that the four RF sensors have the best quantum correlation properties. Each RF sensor encompasses an electro-optic modulator (EOM) to convert the probed RF signal into quadrature displacement of infrared light, and a high-efficiency balanced homodyne detector (HOM) to discern the phase shift with sensitivity beyond the shot noise limit. The home-made EOM, whose transmissivity is larger than 99%, ensures low-loss characteristics of quantum state. The amplitude and phase of RF signal are individually manipulated by four clock-synchronized function generators with $\Omega=3$ MHz modulation frequency. To estimate the displacement α_m , a local oscillator and the sensing beam are overlapped at a 50:50 BS with an interference efficiency of 99.9%. The output of 50:50 BS is detected by home-made balanced homodyne detector (HOM), whose common mode rejection ratio is 75 dB and quantum efficiency is larger than 99%. For each sensor, the relative phase between local oscillator and sensing beam is controlled to $\pi/2$, observing the phase quadrature of sensing beam.

The output of four HOMs through the same four bandpass filters from 1.8 MHz to 4.5 MHz are demodulated with 3 MHz from another channel of the clock-synchronized function generator. The phases of demodulation signal are meticulously adjusted to compensate the circuit latency caused by various electronic components. After amplified by a low-noise and high-gain amplifier, the time-domain data are recorded by four-channel oscilloscope and post-processed to estimate the amplitude and phase information of RF signal.

4. Experimental results

To pre-estimate the RF signal, the four-sensor network (X_0, X_1, X_2 , and X_3) is arranged in a linear topology, and the first, second and third derivatives of radio-frequency (RF) phase at edge sensor X_0 can be estimated with the respective optimum weights. In order to enhance the sensitivity of the first derivative, we estimate the phase $\varphi = \sum_{j=0}^3 \beta_j \varphi_j$

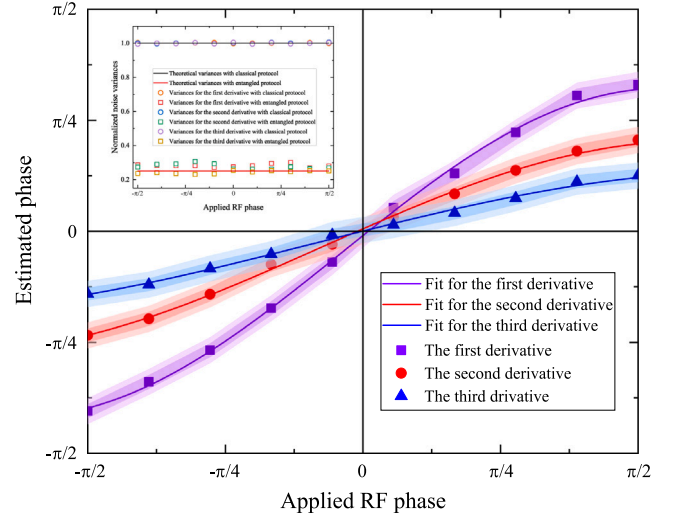


Fig. 3. Estimated phase for each-order derivatives versus applied RF phase at an edge sensor. The curves and data points show the theoretical fitting and experimental results. All signals are normalized using the same factor for the SQL normalization. The shaded area shows the normalized standard deviation for the entangled (dark color) and classical separable (light color) sensor networks. Inset: normalized noise variances for classical and entangled protocols. Circles: measured noise variances with classical separable network; squares: measured noise variances with entangled network; black line: theoretical prediction for classical protocol; red line: theoretical prediction for entangled protocol in the presence of loss.

with optimum weights $\beta_0 : \beta_1 : \beta_2 : \beta_3 = -11/6 : 3 : -3/2 : 1/3$ by setting the splitting ratio of VBSs to be 27.5:72.5, 62:38 and 82:18. The negative signs in the weights are introduced by adding a π -phase delay in the corresponding optical path. The pink curve in Fig. 3 shows the measured noise powers of the first derivative with different applied RF phase. An almost invariable squeezing level of -5.2 ± 0.1 dB for the first derivative is implemented in the experiment, allowing arbitrary phase estimation with enhanced sensitivity. Analogously, the optimum weights for estimating the second (third) derivative are $\beta_0 : \beta_1 : \beta_2 : \beta_3 = 2 : -5 : 4 : -1$ ($-1 : 3 : -3 : 1$), the corresponding splitting ratios of the VBSs are 17:83, 50:50 and 80:20 (12.5:87.5, 43:57 and 75:25). The reduced noise power of -5.5 ± 0.1 dB (-5.9 ± 0.1 dB) for the second derivative (third one) is experimentally obtained, respectively. The inset of Fig. 3 represents the normalized noise variances for both protocols, from which the quantum advantage with entangled network is obviously observed. With the optimum weights for each sensor, the estimation sensitivity is limited by the auxiliary phase squeezed state and experimental loss. Considering the optical loss of three half-wave plates and three polarization beam splitters (6%), and the optical loss of electro-optic phase modulator (1.5%), the theoretical predicted noise variances with four-partite entangled states are reduced to 25% of that with the classical protocols.

Supposed the distance between the edge sensor X_0 and other sensor X_m can be expressed as $\Delta x_m = m * \Delta x$, where Δx is the distance between two adjacent sensors, and m represents the distance gain. According to the theoretical results, the relationship between the relative phase shift $\varphi_m - \varphi_0$ and the distance gain m is expressed as

$$\varphi_m - \varphi_0 = \varphi_0' \Delta x * m + \frac{1}{2} \varphi_0'' \Delta x^2 * m^2 + \frac{1}{6} \varphi_0''' \Delta x^3 * m^3 \quad (3)$$

On the grounds of the first, second and third derivatives of the RF phase at edge sensor, we pre-estimate the displacement amplitude for arbitrary sensor, shown in Fig. 4. The shaded area showcases the pre-estimation uncertainties for the classical (light blue) and entangled (dark blue) sensor networks. Apparently, the pre-estimation uncertainties of RF signal for arbitrary sensor can be reduced by the introduction of quantum technology. The inserted figure represents

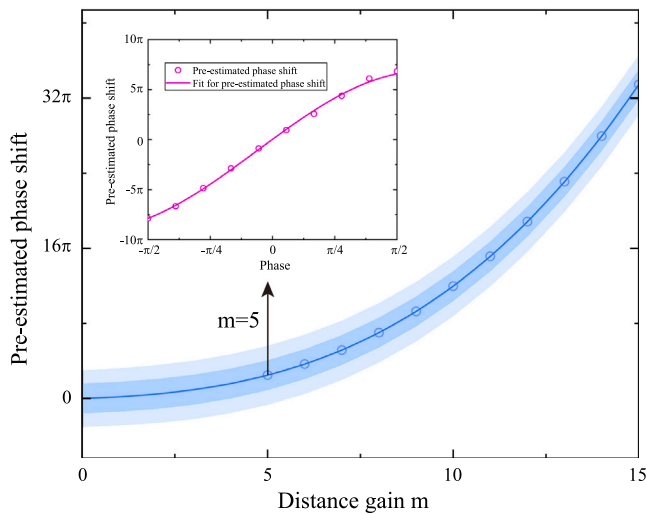


Fig. 4. Theoretical pre-estimation of phase shift for arbitrary sensor as a function of distance gain m . The curve shows the numerical results of estimated phase shift for arbitrary sensor arranged in linear topology. Shaded area: estimation uncertainties for the entangled (dark blue) and classical (light blue) sensor networks. The inserted figure represents the pre-estimated phase shift for the fifth sensor.

the pre-estimated phase shift for the fifth sensor, which follows a sinusoidal distribution. As stated above, the accurate phase estimation can be achieved with at least three derivatives. In contrast to previous literatures that estimates the phase shift by employing only the first derivative of RF signal, this work, exploiting higher-order derivatives and quantum enhancement protocol, pre-estimates the AoA with an enhanced sensitivity of nearly 49.5%. Assuming that the distance Δx is 1 km, then the phase shift of the fifth sensors is $\pi/4$, the corresponding AoA is 1.418.

5. Conclusion

In conclusion, we have experimentally demonstrated the quantum-enhanced AoA pre-estimation of RF signals via continuous variable four-partite entanglement network. By utilizing the optimum weights, the first, second, and third derivatives of RF phase at edge sensor are directly observed with a noise reduction of above -5.2 dB. As stated above, three-order Taylor expansion polynomial can estimate the phase shift with a low uncertainty. In combination with the quantum enhancement, the uncertainty of the AoA pre-estimation is further improved. Utilizing the AoA pre-estimation results, we expect to predict the target orientation, which conduces to both shorten scanning time and improve processing efficiency of a large-scale sensor array.

Declaration of competing interest

The authors declare that there is no conflict of interests.

Data availability

Data will be made available on request.

Acknowledgment

This work has been approved for submission by all authors and has not been published or submitted for publication elsewhere.

Funding

National Natural Science Foundation of China (NSFC) (Grants No. 62225504, No. 62027821, No. 62035015, No. 12174234, No. 11874250, No. U22A6003, No. 12274275); the National Key R&D Program of China (Grant No. 2020YFC2200402); Key R&D Program of Shanxi, China (Grant No. 202102150101003); Program for Sanjin Scholar of Shanxi Province.

References

- [1] V. Giovannetti, S. Lloyd, L. Maccone, Advances in quantum metrology, *Nature Photonics* 5 (4) (2011) 222–229.
- [2] V. Giovannetti, S. Lloyd, L. Maccone, Quantum metrology, *Phys. Rev. Lett.* 96 (2006) 010401.
- [3] L. Pezzer, A. Smerzi, M.K. Oberthaler, R. Schmied, P. Treutlein, Quantum metrology with nonclassical states of atomic ensembles, *Rev. Modern Phys.* 90 (3) (2018) 035005.
- [4] M. Zwiernik, C.A. Pérez-Delgado, P. Kok, General optimality of the Heisenberg limit for quantum metrology, *Phys. Rev. Lett.* 105 (18) (2010) 180402.
- [5] V. Giovannetti, S. Lloyd, L. Maccone, Quantum-enhanced measurements: Beating the standard quantum limit, *Science* 306 (5700) (2004) 1330–1336.
- [6] B. Escher, R. de Matos Filho, L. Davidovich, General framework for estimating the ultimate precision limit in noisy quantum-enhanced metrology, *Nat. Phys.* 7 (5) (2011) 406–411.
- [7] C.M. Caves, Quantum-mechanical noise in an interferometer, *Phys. Rev. D* 23 (8) (1981) 1693.
- [8] H. Katori, Optical lattice clocks and quantum metrology, *Nature Photonics* 5 (4) (2011) 203–210.
- [9] C.F. Roos, M. Chwalla, K. Kim, M. Riebe, R. Blatt, ‘Designer atoms’ for quantum metrology, *Nature* 443 (7109) (2006) 316–319.
- [10] N. Borgohain, S. Konar, Broadband mid-infrared supercontinuum generation in three-level multiple quantum wells using short optical pulses, *Opt. Laser Technol.* 120 (2019) 105684.
- [11] T. Macrì, A. Smerzi, L. Pezzer, Loschmidt echo for quantum metrology, *Phys. Rev. A* 94 (1) (2016) 010102.
- [12] M. Von Helversen, J. Böhm, M. Schmidt, M. Gschrey, J.-H. Schulze, A. Strittmatter, S. Rodt, J. Beyer, T. Heindel, S. Reitzenstein, Quantum metrology of solid-state single-photon sources using photon-number-resolving detectors, *New J. Phys.* 21 (3) (2019) 035007.
- [13] W. Wang, Y. Wu, Y. Ma, W. Cai, L. Hu, X. Mu, Y. Xu, Z.-J. Chen, H. Wang, Y. Song, et al., Heisenberg-limited single-mode quantum metrology in a superconducting circuit, *Nature Commun.* 10 (1) (2019) 1–6.
- [14] B. Li, B. Yuan, C. Chen, X. Xiang, R. Quan, R. Dong, S. Zhang, R.-B. Jin, Spectrally resolved two-photon interference in a modified Hong–Ou–Mandel interferometer, *Opt. Laser Technol.* 159 (2023) 109039.
- [15] R. Schnabel, N. Mavalvala, D.E. McClelland, P.K. Lam, Quantum metrology for gravitational wave astronomy, *Nature Commun.* 1 (1) (2010) 1–10.
- [16] B.-B. Li, J. Bilek, U.B. Hoff, L.S. Madsen, S. Forstner, V. Prakash, C. Schäfermeier, T. Gehring, W.P. Bowen, U.L. Andersen, Quantum enhanced optomechanical magnetometry, *Optica* 5 (7) (2018) 850–856.
- [17] M. Zhou, X. Cao, Y. Lu, Y. Wang, Y. Bao, Z. Jia, Y. Fu, H. Yin, Z. Chen, Experimental quantum advantage with quantum coupon collector, *Research* 2022 (2022) 9798679.
- [18] W. Liu, C. Li, Y. Xie, C. Weng, J. Gu, X. Cao, Y. Lu, B. Li, H. Yin, Z. Chen, Homodyne detection quadrature phase shift keying continuous-variable quantum key distribution with high excess noise tolerance, *PRX Quantum* 2 (2021) 040334.
- [19] N. Mirkin, M. Larocca, D. Wisniacki, Quantum metrology in a non-Markovian quantum evolution, *Phys. Rev. A* 102 (2) (2020) 022618.
- [20] A.J. Brady, C. Gao, R. Harnik, Z. Liu, Z. Zhang, Q. Zhuang, Entangled sensor-networks for dark-matter searches, *PRX Quantum* 3 (2022) 030333.
- [21] H. Shi, Z. Zhang, S. Pirandola, Q. Zhuang, Entanglement-assisted absorption spectroscopy, *Phys. Rev. Lett.* 125 (2020) 180502.
- [22] F. Laghezza, F. Scotti, P. Ghelfi, A. Bogoni, Photonics-assisted multiband RF transceiver for wireless communications, *J. Lightwave Technol.* 32 (16) (2014) 2896–2904.
- [23] P. Ghelfi, F. Laghezza, F. Scotti, G. Serafino, A. Capria, S. Pinna, D. Onori, C. Porzi, M. Scaffardi, A. Malacarne, et al., A fully photonics-based coherent radar system, *Nature* 507 (7492) (2014) 341–345.
- [24] Y. Yuan, W. Yi, L. Kong, Joint tracking sequence and dwell time allocation for multi-target tracking with phased array radar, *Signal Process.* 192 (2022) 108374.
- [25] P. Li, L. Yan, J. Ye, X. Feng, W. Pan, B. Luo, X. Zou, T. Zhou, Z. Chen, Photonic approach for simultaneous measurements of Doppler-frequency-shift and angle-of-arrival of microwave signals, *Opt. Express* 27 (6) (2019) 8709–8716.

- [26] Z. Cao, Q. Wang, R. Lu, H. Van den Boom, E. Tangdiongga, A. Koonen, Phase modulation parallel optical delay detector for microwave angle-of-arrival measurement with accuracy monitored, *Opt. Lett.* 39 (6) (2014) 1497–1500.
- [27] H. Zhuo, A. Wen, Y. Wang, Photonic angle-of-arrival measurement without direction ambiguity based on a dual-parallel Mach-Zehnder modulator, *Opt. Commun.* 451 (2019) 286–289.
- [28] H. Chen, E.H.W. Chan, Angle-of-arrival measurement system using double RF modulation technique, *IEEE Photonics J.* 11 (1) (2018) 1–10.
- [29] H. Chen, C. Huang, E.H.W. Chan, Photonic approach for measuring AOA of multiple signals with improved measurement accuracy, *IEEE Photonics J.* 12 (3) (2020) 1–10.
- [30] X. Zou, W. Li, W. Pan, B. Luo, L. Yan, J. Yao, Photonic approach to the measurement of time-difference-of-arrival and angle-of-arrival of a microwave signal, *Opt. Lett.* 37 (4) (2012) 755–757.
- [31] H. Chen, E.H. Chan, Simple approach to measure angle of arrival of a microwave signal, *IEEE Photonics Technol. Lett.* 31 (22) (2019) 1795–1798.
- [32] Y. Xia, W. Li, W. Clark, D. Hart, Q. Zhuang, Z. Zhang, Demonstration of a reconfigurable entangled radio-frequency photonic sensor network, *Phys. Rev. Lett.* 124 (15) (2020) 150502.
- [33] L. Zhang, J.Q. Gan, H. Wang, Localization of neural efficiency of the mathematically gifted brain through a feature subset selection method, *Cogn. Neurodyn.* 9 (5) (2015) 495–508.
- [34] G. Vinci, S. Lindner, F. Barbon, R. Weigel, A. Koelpin, Promise of a better position, *IEEE Microw. Mag.* 13 (7) (2012) S41–S49.
- [35] X. Guo, C.R. Breum, J. Borregaard, S. Izumi, M.V. Larsen, T. Gehring, M. Christandl, J.S. Neergaard-Nielsen, U.L. Andersen, Distributed quantum sensing in a continuous-variable entangled network, *Nat. Phys.* 16 (3) (2020) 281–284.
- [36] Z. Zhang, Q. Zhuang, Distributed quantum sensing, *Quant. Sci. Technol.* 6 (4) (2021) 043001.
- [37] Q. Zhuang, Z. Zhang, J.H. Shapiro, Distributed quantum sensing using continuous-variable multipartite entanglement, *Phys. Rev. A* 97 (2018) 032329.
- [38] S. Shi, L. Tian, Y. Wang, Y. Zheng, C. Xie, K. Peng, Demonstration of channel multiplexing quantum communication exploiting entangled sideband modes, *Phys. Rev. Lett.* 125 (2020) 070502.
- [39] W. Yang, S. Shi, Y. Wang, W. Ma, Y. Zheng, K. Peng, Detection of stably bright squeezed light with the quantum noise reduction of 12.6 dB by mutually compensating the phase fluctuations, *Opt. Lett.* 42 (21) (2017) 4553–4556.
- [40] X. Sun, Y. Wang, Y. Tian, Q. Wang, L. Tian, Y. Zheng, K. Peng, Deterministic and universal quantum squeezing gate with a teleportation-like protocol, *Laser Photonics Rev.* (2021) 2100329.
- [41] S. Shi, Y. Wang, L. Tian, W. Li, Y. Wu, Q. Wang, Y. Zheng, K. Peng, Continuous variable quantum teleportation network, *Laser Photonics Rev.* (2022) 2200508.